RSC Advances

PAPER

View Article Online
View Journal | View Issue

Cite this: *RSC Adv.*, 2024, **14**, 6262

New insight into the plastic deformation mechanisms during the SiO_2 phase transition process†

Zhenlun Wei,[a] Yubiao Li, *[ab] Peiyue Li,[cd] Li Pan,[d] Wanqing Li,[a] Xianglin Hu[a] and Yunxiang Gu[a]

Received 8th November 2023
Accepted 19th January 2024

DOI: 10.1039/d3ra07633d

rsc.li/rsc-advances

The removal of lattice impurities is the key to the purification of high-purity quartz (HPQ), especially for the intracell lattice impurities. Generally, the intracell lattice impurities can be migrated to the quartz surface *via* roasting, then removed by acid leaching. In order to reveal the phase transition of quartz during the roasting process, the evolution of structure, bond length, volume, lattice parameter and lattice stress in original, Ti^{4+}, Al^{3+}/Li^{+} and $4H^{+}$ substituted SiO_2 phases were employed to investigate the mechanisms of plastic deformation based on density functional theory calculations. Results showed that the evolution of bond lengths and volumes were mainly dominated by phase transition, and the interstitial volume in high temperature SiO_2 phases was higher than that in low temperature, indicating that the phase transition from α-quartz to β-cristobalite was beneficial to the migration of interstitial impurities. In addition, the phase transition from α-quartz to β-cristobalite needs to overcome the energy barriers while the phase transition from α-cristobalite to β-cristobalite needs to overcome the lattice stress. This study therefore provides an excellent theoretical basis for the plastic deformation mechanism, for the first time, beneficial to understanding the removal mechanisms of lattice impurities.

1 Introduction

The quartz crucible prepared using high-purity quartz (HPQ) is a necessary container for monocrystalline silicon,[1,2] significantly influencing the healthy development of semiconductors, 5G communications, new energy and other industrial fields.[3] The key to the purification of HPQ, especially for 5N HPQ (SiO_2 content ≥ 99.999%) is to remove the lattice impurities.[4–6] Normally, the lattice impurities can be divided into lattice substitution impurity and lattice interstitial impurities based on their location.[7,8] In terms of substitution configuration of a single Si atom, lattice impurities can be divided into three kinds, *i.e.*, simple substitution (such as the substitution of Si^{4+} by Ti^{4+}), substitution with interstitial charge compensator (such as the substitution of Si^{4+} by Al^{3+}/Li^{+}), and silanol groups (the substitution of Si^{4+} by $4H^{+}$).[9–13]

Generally, the lattice impurities can be removed *via* roasting and leaching process.[10,14–16] Within which, the leaching process can only remove the surface impurities,[10] while the lattice impurities can migrate from the intracell to surface during high-temperature roasting process. For instance, Wei *et al.*[16] investigated the migration mechanisms during phase transition from α-quartz to β-quartz, suggesting that the lattice impurity of Al^{3+} and Li^{+} migrated from intracell to quartz sand surface *via* the *c* axis. Wu *et al.*[17] indicated that the lattice impurities of Al^{3+}, Fe^{3+}, K^{+} and Ti^{4+} migrated from intracell to surface during the NH_4Cl roasting process.

In addition, quartz normally undergoes phase transition process during roasting. Götze *et al.*[18] reported 15 polymorph SiO_2 phases, *e.g.*, the most common phases were α-quartz, β-quartz, β-cristobalite and α-cristobalite, *etc.* The phase transition from α-quartz to β-quartz, from β-quartz to β-cristobalite and from β-cristobalite to α-cristobalite occurred at 573 °C, 1470 °C and 270 °C, respectively.[19–23] However, the plastic deformation mechanisms during these phase transitions were still unclear, which significantly affected the properties of SiO_2 lattice and the removement of lattice impurities. For instance, Wei *et al.*[16] indicated that the interstitial volume was increased during the phase transition from α-quartz to β-quartz, beneficial to the migration of lattice interstitial impurities, such as Li^{+}. Blankenburg *et al.*[24] found that the defects or twinning formed during the phase transition from α-quartz to β-quartz influenced the distribution of lattice impurities.

[a]*School of Resources and Environmental Engineering, Wuhan University of Technology, 122, Luoshi Road, Hongshan District, Wuhan 430070, Hubei, China. E-mail: yubiao.li@whut.edu.cn*

[b]*Key Laboratory of Green Utilization of Critical Non-metallic Mineral Resources, Ministry of Education, Wuhan 430070, Hubei, China*

[c]*National Innovation Center for Advanced Glass Materials, Bengbu, Anhui, 233018, PR China*

[d]*CNBM Research Institute for Advanced Glass Materials Group Co., Ltd, Bengbu, 233018, PR China*

† Electronic supplementary information (ESI) available. See DOI: https://doi.org/10.1039/d3ra07633d

In this case, the phase transition of original and substitution SiO_2 phases were employed to investigate the plastic deformation mechanism during roasting process based on the density functional theory (DFT) calculation. Specifically, α-quartz, β-quartz, β-cristobalite and α-cristobalite were considered as the original SiO_2 phases, and Ti^{4+}, Al^{3+}/Li^{+} and $4H^{+}$ were considered as the impurity ion substituted in the crystal of quartz. This study, for the first time, clearly revealed the evolution of structure, bond length, volume, lattice parameter, lattice stress and energy in original, and substituted (Ti^{4+}, Al^{3+}/Li^{+} and $4H^{+}$) SiO_2 phases, therefore providing an excellent theoretical basis for the plastic deformation during the phase transition process, beneficial to understanding the removal mechanisms of lattice impurities.

2 Methodology

Similar to our previous research,[16] the generalized gradient approximation (GGA) with PW91 correlation potential was considered to perform the DFT calculation through Materials Studio in CASTEP package.[25] A kinetic energy cutoff of 360 eV was chosen for the geometric optimization calculation, and the Monkhorst–Pack scheme *k*-point meshes were 3 × 3 × 4, 2 × 2 × 3, 1 × 2 × 2 and 1 × 1 × 2 for α-quartz, β-quartz, β-cristobalite and α-cristobalite. The interstitial volume was calculated through the methods in our previous research.[16] And the lattice stress was calculated *via* eqn (1):[26,27]

$$S_L = -B \times (\Delta V/V) \quad (1)$$

where S_L, B and V were the lattice stress, bulk modulus and bulk volume of SiO_2 phases, ΔV was the bulk volume changes between SiO_2 phases. The formation energy was calculated *via* eqn (2):[28]

$$E_f = E_{tol} - aE_{Si} - bE_O - cE_{Ti} - dE_{Al} - eE_{Li} - fE_H \quad (2)$$

where E_f was the formation energy, E_{tol} was the total energy of SiO_2 phase, a, b, c, d, e and f were the numbers of Si, O, Ti, Al, Li and H atoms in SiO_2 phase, respectively. E_{Si}, E_O, E_{Ti}, E_{Al}, E_{Li} and E_H were the energies of the constituents in their ambient-condition ground-state phases for Si, O, Ti, Al, Li and H atoms, respectively.

3 Results and discussion

3.1 Structure of original SiO_2 phases

In order to better compare the plastic deformation mechanisms between typical SiO_2 phases, the supercells with the same number of atoms (all in 72 atoms) of 2 × 2 × 2 α-quartz, 2 × 2 × 2 β-quartz, 3 × 1 × 1 β-cristobalite and 3 × 2 × 1 α-cristobalite were employed to perform the geometric optimization calculation, and the optimized structures were shown in Fig. 1.

These typical SiO_2 phases had similar arrangement of atoms, *e.g.*, each Si atom was boned with four surrounding O atoms to form a silica tetrahedron (*i.e.*, four Si–O bonds), and each O atom was boned with two surrounding Si atoms to connect silica tetrahedron.[16,29,30] However, the specific Si–O bond length and Si–O–Si angle were different for these typical SiO_2 phases, *i.e.*, the Si–O bond length were 1.619/1.625 Å, 1.614 Å, 1.608 Å and 1.615/1.619 Å in α-quartz, β-quartz, β-cristobalite and α-cristobalite, while the Si–O–Si angle were 153.19°, 144.47°, 180.00° and 153.27°, respectively (Table 1), resulting in different crystal systems for these typical SiO_2 phases, *i.e.*, trigonal,

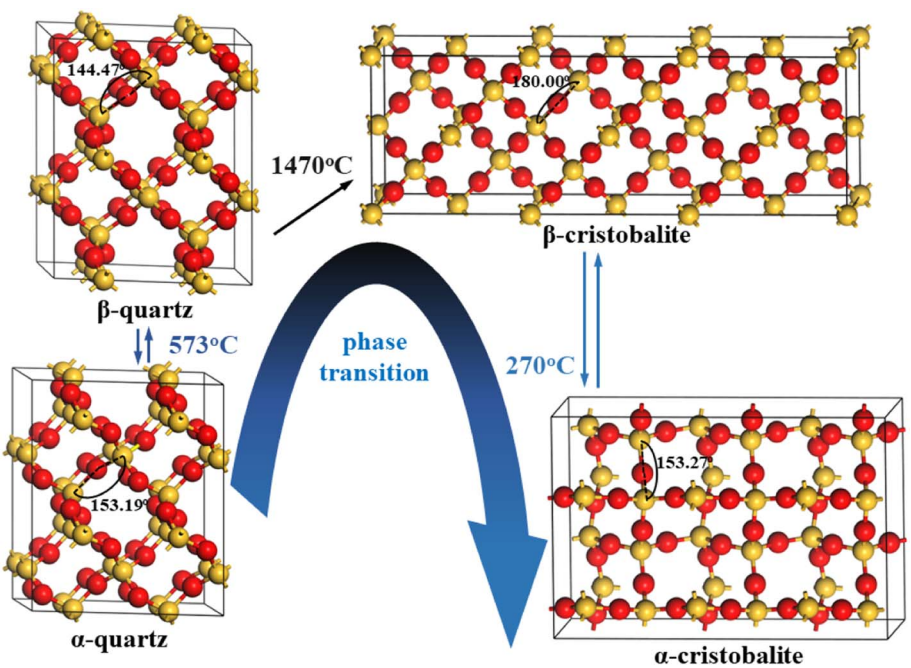

Fig. 1 The structure of optimized typical SiO_2 phases (all in $Si_{24}O_{48}$).

Table 1 Lattice parameters of optimized typical SiO_2 phases

Lattice parameters	α-Quartz	β-Quartz	β-Cristobalite	α-Cristobalite
Supercell size	2 × 2 × 2	2 × 2 × 2	3 × 1 × 1	3 × 2 × 1
Atomic number	72	72	72	72
a (Å)	9.923	10.097	22.278	15.377
b (Å)	9.923	10.097	7.425	10.247
c (Å)	10.945	11.214	7.425	7.141
Volume (Å^3)	933.224	990.088	1228.300	1125.240
Si–O bond (Å)	1.619/1.625	1.614	1.608	1.615/1.619
O–Si–O angle (°)	153.19	144.47	180.00	153.27

hexagonal, cubic and tetragonal for α-quartz, β-quartz, β-cristobalite and α-cristobalite, respectively.[18,20–23]

In addition, the bulk volumes were 933.224 Å^3, 990.088 Å^3, 1228.300 Å^3 and 1125.240 Å^3 for α-quartz, β-quartz, β-cristobalite and α-cristobalite (Table 1), giving an order of bulk volume in β-cristobalite > α-cristobalite > β-quartz > α-quartz, indicating that the bulk volumes in cristobalite phases were greater than that in quartz phases. Moreover, the bulk volume in high temperature SiO_2 phases were higher than that in low temperature SiO_2 phases. In this case, the bulk volume of these typical SiO_2 phases was related to the temperature of the phase transition.

3.2 Evolution of bond length

The substitution of Si^{4+} by Ti^{4+}, Al^{3+}/Li^{+} and $4H^{+}$ were performed to investigate the influence of impurity ion to the plastic deformation process from α-quartz to α-cristobalite. The structures of original and substitution 2 × 2 × 2 α-quartz, 2 × 2 × 2 β-quartz, 3 × 1 × 1 β-cristobalite and 3 × 2 × 1 α-cristobalite were shown in Fig. 2, S1, S2 and S3,† respectively. From Fig. 2, four Ti–O, Al–O and H–O bonds were formed when Si^{4+} was substituted by Ti^{4+}, Al^{3+}/Li^{+} and $4H^{+}$, while the Li in the interstitial of the lattice did not bonded with the surrounding O atoms (Fig. 2(c)). In addition, the changes of structure caused by impurity ion substitution (Fig. 2) were significant smaller than that caused by phase transition (Fig. 1), the impurity substitution only affected the length of the surrounding Si–O bonds. Similar structure changes were observed in β-quartz, β-cristobalite and α-cristobalite, thus the bond lengths in these original and substitution typical SiO_2 phases were investigated to clarify the plastic deformation caused by impurity ion substitution and phase transition.

The average bond lengths of Si–O, Ti–O, Al–O and H–O bonds in original and substituted SiO_2 phases were shown in Fig. 3. Overall, the average bond lengths were in an order of Ti–O > Al–O > Si–O > H–O bonds, since the ionic radius for Ti^{4+}, Al^{3+}, Si^{4+} and H^{+} were 0.61 Å, 0.54 Å, 0.40 Å and 0.24 Å.[18,31] For the Si–O bonds, the average Si–O bond lengths for α-quartz, β-quartz, β-cristobalite and α-cristobalite in the original phases were 1.622 Å, 1.614 Å, 1.608 Å and 1.617 Å, respectively. It was clearly that the average Si–O bond lengths in β-quartz (or β-cristobalite) were shorter than that in α-quartz (or α-cristobalite).[16] Same evolution rules for average Si–O bond lengths were presented in Ti^{4+}, Al^{3+}/Li^{+} and $4H^{+}$ substituted SiO_2 phases, indicating that the average Si–O bond lengths in high temperature were shorter than that in

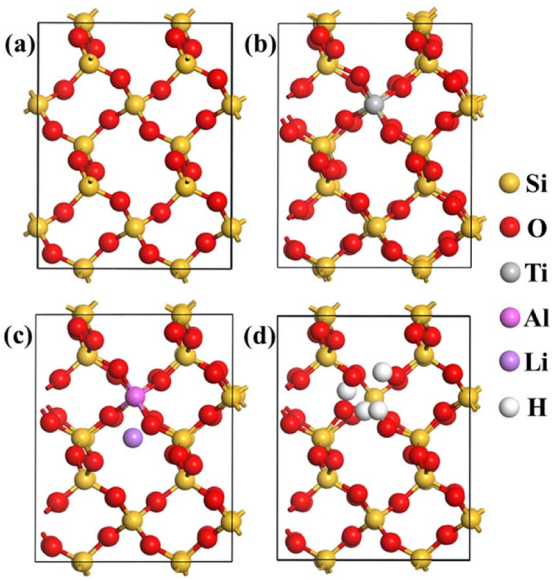

Fig. 2 Structures of optimized original and Ti^{4+}, Al^{3+}/Li^{+} and $4H^{+}$ substituted 2 × 2 × 2 α-quartz supercells: (a) $Si_{24}O_{48}$; (b) $Si_{23}TiO_{48}$; (c) $Si_{23}AlLiO_{48}$; (d) $Si_{23}H_4O_{48}$.

low temperature for all original and substituted SiO_2 phases. In addition, the average Si–O bond length changes caused by phase transition were more significant than that due to substitution, *e.g.*, the changes caused by the phase transition were −0.008 Å (*i.e.*, 1.614–1.622 Å), −0.014 Å (*i.e.*, 1.608–1.622 Å) and −0.005 Å (*i.e.*, 1.617–1.622 Å) from α-quartz to β-quartz, β-cristobalite and α-cristobalite, respectively, while caused by Ti^{4+}, Al^{3+}/Li^{+} and $4H^{+}$ substitution for α-quartz were −0.002 Å (*i.e.*, 1.620–1.622 Å), 0.002 Å (*i.e.*, 1.624–1.622 Å) and −0.004 Å (*i.e.*, 1.618–1.622 Å), respectively (Fig. 3(a)).

The evolution rules of Al–O and H–O bonds were similar to Si–O bonds during the plastic deformation process, *i.e.*, the average bond lengths in high temperature SiO_2 phases were shorter than that in low temperature. However, the evolution rule was only applied to the phase transition of α-quartz to β-quartz for the Ti–O bonds. In contrast, the average Ti–O bond length in β-cristobalite was longer than that in α-cristobalite, *i.e.*, the average Ti–O bond lengths were 1.812, 1.800, 1.805 and 1.787 Å for Ti^{4} substitution α-quartz, β-quartz, β-cristobalite and α-cristobalite, respectively, may due to the higher fusion point of Ti than Si and Al (*i.e.*, 1668 °C, 1410 °C and 660 °C for Ti, Si and Al). Overall, the

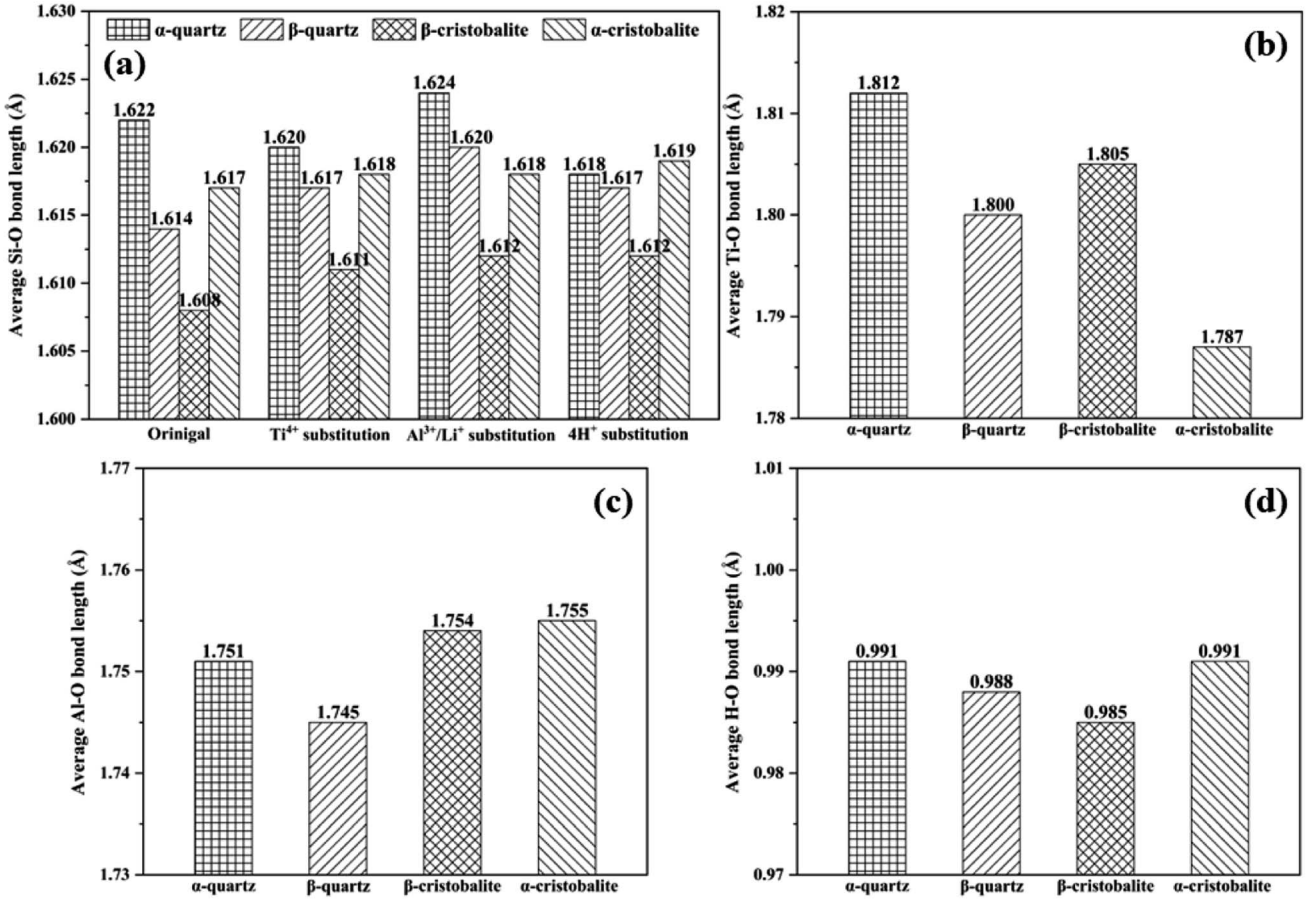

Fig. 3 Average bond length of original and substituted SiO_2 phases: (a) Si–O bonds; (b) Ti–O bonds; (c) Al–O bonds; (d) H–O bonds.

evolution of bond length was mainly dominated by phase transition rather than impurity ion substitution.

3.3 Evolution of volume

Fig. 4 showed the bulk and interstitial volume of original and substituted SiO_2 phases. Both the phase transition and the impurity ion substitution increased the bulk volume. Similar to the original SiO_2 phases as discussed in Section 3.1, the bulk volumes for the phase transformed SiO_2 phases were larger than that of the ion substituted phase, giving an order of bulk volume in β-cristobalite > α-cristobalite > β-quartz > α-quartz, further indicating greater bulk volume in high temperature SiO_2 phases than that in low temperature for all SiO_2 phases. For instance, the bulk volume changes caused by phase transition were 56.864 Å^3 (*i.e.*, 990.088–933.224 Å^3), 295.076 Å^3 (*i.e.*, 1228.300–933.224 Å^3) and 192.016 Å^3 (*i.e.*, 1125.240–933.224 Å^3) from α-quartz to β-quartz, α-cristobalite and β-cristobalite, while the bulk volume changes caused by Ti^{4+}, Al^{3+}/Li^+ and $4H^+$ substitution for α-quartz were 43.336 Å^3 (*i.e.*, 976.560–933.224 Å^3), 51.130 (*i.e.*, 984.354–933.224 Å^3) and 55.651 Å^3 (*i.e.*, 988.875–933.224 Å^3), respectively. In this case, the evolution of bulk volume was mainly dominated by phase transition rather than substitution due to impurity ions.

The interstitial volume was closely related to the migration of interstitial impurity such as Li^+, Na^+, K^+, *etc.*[16] Thus the evolution of interstitial volume was calculated (Fig. 4(b)). Similar to the evolution of bulk volume, the interstitial volume changes caused by phase transition were more significant than that by impurity ion substitution, *e.g.*, the interstitial volume changes caused by phase transition were 59.049 Å^3 (*i.e.*, 937.000–877.951 Å^3), 299.133 Å^3 (*i.e.*, 1177.084–877.951 Å^3) and 194.969 Å^3 (*i.e.*, 1072.920–877.951 Å^3) from α-quartz to β-quartz, α-cristobalite and β-cristobalite, respectively, while caused by Ti^{4+}, Al^{3+}/Li^+ and $4H^+$ substitution for α-quartz were 47.232 Å^3 (*i.e.*, 925.183–877.951 Å^3), 53.968 Å^3 (*i.e.*, 931.919–877.951 Å^3) and 61.267 Å^3 (*i.e.*, 939.218–877.951 Å^3), respectively (Fig. 3(b)). These indicated that the evolution of interstitial volume was mainly dominated by phase transition rather than substitution due to impurity ions.

In addition, the interstitial volume changes caused by the phase transition was greater than that of bulk volume, possibly due to bigger bulk volume and shorter average bond lengths for the high temperature SiO_2 phases. Moreover, the interstitial volume change from β-quartz to α-cristobalite was significant greater than that from α-quartz to β-quartz, *i.e.*, 240.084 Å^3 (*i.e.*, 1177.084–937.000 Å^3) *vs.* 59.049 Å^3, indicating that the migration of interstitial impurities was proportional to temperature.[16]

3.4 Evolution of lattice parameter

Since the evolution of bulk volume was mainly dominated by phase transition, the changes of lattice parameters (Δa_i, Δb_i and

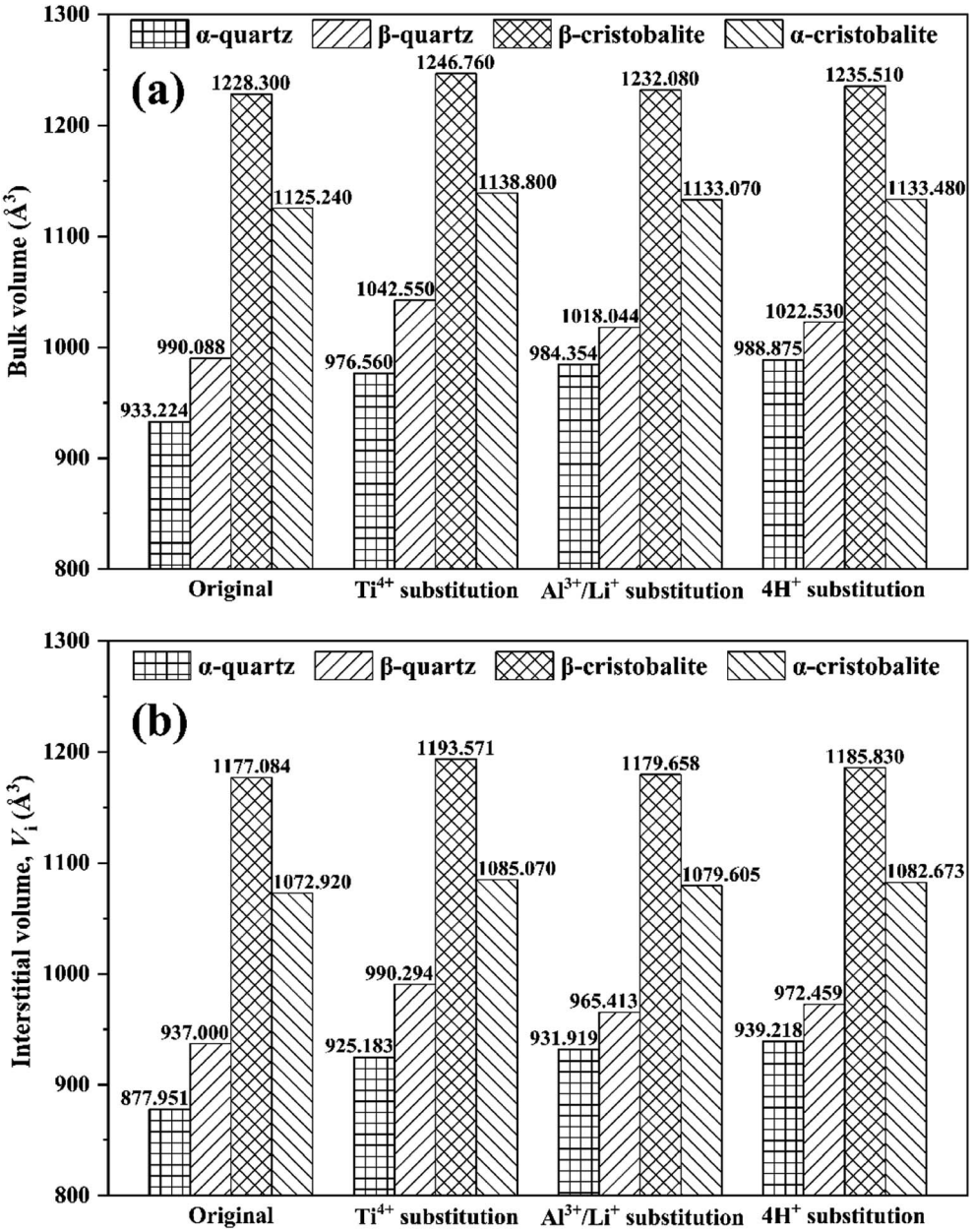

Fig. 4 (a) Bulk volume and (b) interstitial volume of original and substituted SiO_2 phases during phase transition process.

Δc_i) were employed to evaluate the contribution of lattice parameters to the changes of bulk volume (ΔV). As shown in Fig. 5(a) the Δa_i increased with the increase of ΔV for original SiO_2 phases, while Δb_i and Δc_i decreased with the increased ΔV, indicating that Δa_i positively contributed to the increase of bulk volume. In contrast, Δb_i and Δc_i exhibited negative contributes. The values of $\Delta a_i/\Delta V$, $\Delta b_i/\Delta V$ and $\Delta c_i/\Delta V$ of 0.0370, −0.0052 and −0.0138 indicated that the bulk volume of original SiO_2 phases were increased *via a* axis, but decreased mainly *via c* axis during the phase transition process.[26]

Similar contribution rules were observed for Ti^{4+}, Al^{3+}/Li^+ and $4H^+$ substitution, *i.e.*, the bulk volume of substituted SiO_2 phases increased *via a* axis, but decreased mainly *via c* axis during the phase transition process. In this case, the substitution of impurity ion did not change the contribution rule between lattice parameters to bulk volume, but changing the specific $\Delta a_i/\Delta V$, $\Delta b_i/\Delta V$ and $\Delta c_i/\Delta V$ values. For instance, the $\Delta a_i/\Delta V$ values in Ti^{4+}, Al^{3+}/Li^+ and $4H^+$ substituted SiO_2 phases (*i.e.*, 0.0404, 0.0446 and 0.0458, respectively) were greater than that of original SiO_2 phases (*i.e.*, 0.0370), giving a $\Delta a_i/\Delta V$ value order in $4H^+ > Al^{3+}/Li^+ > Ti^{4+}$ > original SiO_2 phases. Same orders were observed for the absolute values of $\Delta b_i/\Delta V$ and $\Delta c_i/\Delta V$, indicating that the contribution of lattice parameters to bulk volumes was related to the number of substitution atoms.

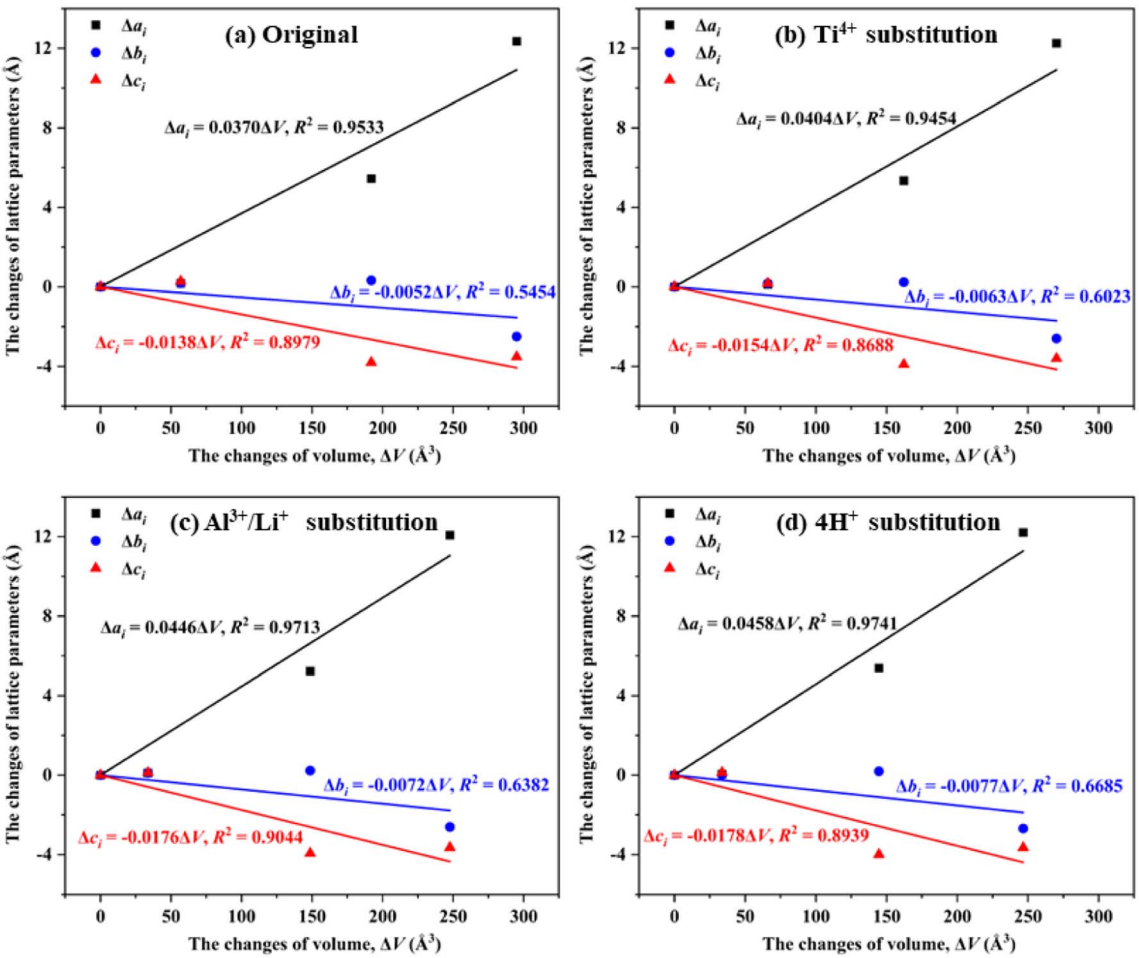

Fig. 5 The contribution of Δa_i, Δb_i and Δc_i to ΔV in (a) original, (b) Ti^{4+} substituted, (c) Al^{3+}/Li^{+} substituted and (d) $4H^{+}$ substituted SiO_2 phases.

3.5 Evolution of lattice stress

Normally, the change of bulk volume needs to overcome the lattice stress, thus lattice stress of original and substituted SiO_2 phases were calculated based on eqn (1). Overall, the lattice stresses were negative for original and substituted β-quartz and β-cristobalite (Fig. 6), but positive for α-cristobalite, *e.g.*, the lattice stresses were −10.521 GPa, −34.095 GPa and 6.740 GPa for original β-quartz, β-cristobalite and α-cristobalite, indicating that the phase transition from α-quartz to β-quartz and from β-quartz to α-cristobalite occurred spontaneously. However, the evolution from α-cristobalite to β-cristobalite needs to overcome lattice stress.

Furthermore, the substitution of impurity ion did not change the lattice stress of SiO_2 phases during the phase transition process, but changing the specific lattice stress values. For instance, the lattice stresses for original, Ti^{4+}, Al^{3+}/Li^{+} and $4H^{+}$ substituted β-quartz were −10.521 GPa, −19.246 GPa, −8.454 GPa and −12.356 GPa, respectively, indicating that the substitution of Ti^{4+} and $4H^{+}$ drived the phase transition from α-quartz to β-quartz easily. However, the substitution of Al^{3+}/Li^{+} occurred difficultly. Differently, the substitution of Ti^{4+}, Al^{3+}/Li^{+} and $4H^{+}$ promoted the phase transition from β-quartz to α-cristobalite easily. In contrast, the phase transition from α-cristobalite to β-cristobalite need to overcome greater lattice stress due to the substitution of Ti^{4+}, Al^{3+}/Li^{+} and $4H^{+}$.

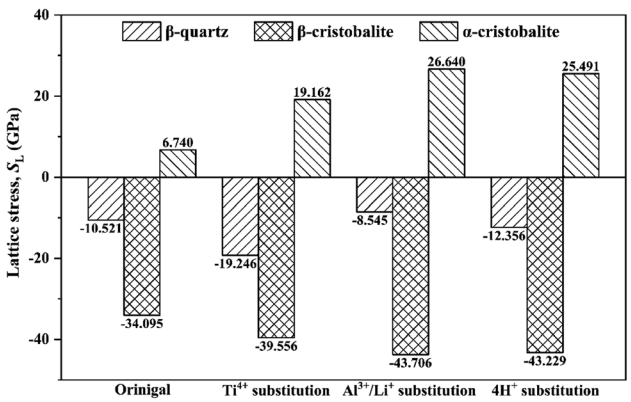

Fig. 6 Lattice stress of original and substituted SiO_2 phases during phase transition. The ΔV used in the lattice stress calculation for β-quartz, β-cristobalite and α-cristobalite were volume changes from α-quartz to β-quartz, from β-quartz to β-cristobalite and from β-cristobalite to α-cristobalite, respectively.

3.6 Evolution of energy

In order to better reveal the energy evolution during the phase transition process, the energy barriers were calculated (Fig. 7(a) and Tables S1–S5†). It was clearly that the energy barriers for β-quartz and β-cristobalite were positive, but negative for α-cristobalite in all SiO_2 phases, *e.g.* the energy barriers were 0.489, 0.333 and −1.973 eV for original β-quartz, β-cristobalite and α-cristobalite, respectively, indicating that the phase transitions from α-quartz to β-quartz and from β-quartz to α-cristobalite need to overcome energy barriers. In contrast, the phase transition from α-cristobalite to β-cristobalite occurred spontaneously from thermodynamic point of view. In other words, the phase transition from α-quartz to β-quartz and further to α-cristobalite were endothermic process but the phase transition from α-cristobalite to β-cristobalite was exothermic process, consistent with the phase transition temperature results shown in Fig. 1.

In addition, the substitution of lattice impurity significantly reduced the energy barriers for the phase transition from α-quartz to β-quartz and further to α-cristobalite, *e.g.*, the energy barriers for original, Ti^{4+}, Al^{3+}/Li^{+} and $4H^{+}$ substituted SiO_2 phases were 0.489, 0.210, 0.147 and 0.115 eV, respectively, indicating that the present of lattice impurities promoted phase transition from thermodynamic point of view.

The formation energy of original and substituted SiO_2 phases were calculated to evaluate the stability of lattice impurity substituted structure (Fig. 7(b)). The original, Ti^{4+} and Al^{3+}/Li^{+} substituted SiO_2 phases exhibited negative formation energies, *e.g.*, −2.798, −4.662 and −2.821 eV for α-quartz phases, respectively. However, $4H^{+}$ substituted SiO_2 phases exhibited positive formation energies, *e.g.*, 9.106 eV for α-quartz, indicating that the original, Ti^{4+} and Al^{3+}/Li^{+} substituted SiO_2 phases can exist stably, while the $4H^{+}$ substituted SiO_2 phases were structurally unstable. In addition, the formation energies were in an order of Ti^{4+} substitution < Al^{3+}/Li^{+} substitution < original

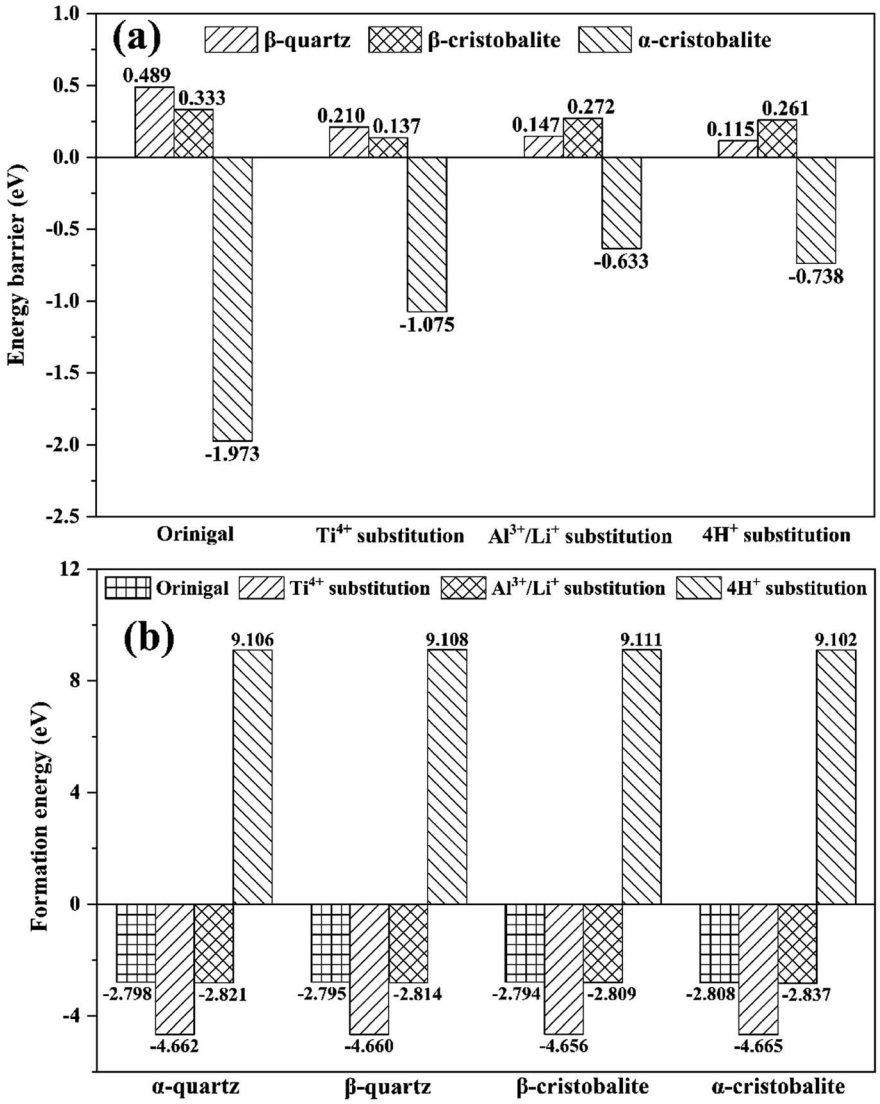

Fig. 7 (a) Energy barrier and (b) formation energy of original and substituted SiO_2 phases during phase transition.

< $4H^+$ substitution. In this case, the lattice impurities Ti and Al were hardly to be removed due to their lower formation energies than that of original SiO_2 phases.[18]

4 Conclusions

This study investigated the plastic deformation mechanisms for the phase transition between α-quartz, β-quartz, β-cristobalite and α-cristobalite based on the evolution of supercell structures, bond lengths, volumes, lattice parameters, lattice stresses and energies in original, Ti^{4+}, Al^{3+}/Li^+ and $4H^+$ substituted SiO_2 phases. Overall, the evolution of bond lengths and volumes were mainly dominated by phase transition rather than substitution due to impurity ions. The average Si–O bond lengths in high temperature SiO_2 phases were shorter than that in low temperature for original and substituted SiO_2 phases. In contrast, the bulk volume in high temperature SiO_2 phases were higher than that in low temperature. Thus, the interstitial volume changes caused by the phase transition was greater than that of the bulk volume, beneficial to the migration of interstitial impurities. In addition, the bulk volume of original and substituted SiO_2 phases increased *via a* axis, but decreased mainly *via c* axis during the phase transition process. In addition, the contribution of lattice parameters to bulk volumes was related to the number of substitution atoms. Moreover, the phase transition from α-quartz to β-quartz and further to α-cristobalite need to overcome energy barriers, while the evolution from α-cristobalite to β-cristobalite needs to overcome a lattice stress.

Author contributions

Methodology, Zhenlun wei, Wanqing Li, Xianglin Hu, software, Zhenlun Wei, Xianglin Hu, Yunxiang Gu, writing—original draft preparation, Zhenlun Wei, Peiyue Li, Li Pan, writing—review and editing, Yubiao Li, supervision, Yubiao Li.

Conflicts of interest

There are no conflicts of interest to declare.

Acknowledgements

The authors would like to acknowledge the financial support from the Key Research and Development Program of Hubei Province (2021BCA127).

References

1 G. K. Warden, M. Juel, B. A. Gaweł and M. Di Sabatino, *Open Ceram.*, 2023, **13**, 100321.
2 M. D. Sabatino, F. W. Thorsen, A. Lanterne, Y. Hu, J. A. Bones and E. Øvrelid, *Energy Technol.*, 2017, 387–394.
3 M. Xia, C. Sun, X. Yang and J. Chen, *Minerals*, 2023, **13**, 261.
4 J. Götze, *Quartz:Deposits, Mineralogy and Analytics*, 2012.
5 J. A. Weil, *Phys. Chem. Miner.*, 1984, **10**, 149–165.
6 B. Perny, P. Eberhardt, K. Ramseyer, J. Mullis and R. Pankrath, *Am. Mineral.*, 1992, **77**, 534–544.
7 R. Stalder, A. Potrafke, K. Billström, H. Skogby, G. Meinhold, C. Gögele and T. Berberich, *Am. Mineral.*, 2017, **102**, 1832–1842.
8 A. Potrafke, R. Stalder, B. C. Schmidt and T. Ludwig, *Contrib. Mineral. Petrol.*, 2019, **174**, 98.
9 A. N. Müller, J. E. Wanvik and P. M. Ihlen, *Springer Geology*, 2012, pp. 71–118.
10 M. Lin, Z. Pei, Y. Li, Y. Liu, Z. Wei and S. Lei, *Miner. Eng.*, 2018, **125**, 42–49.
11 A. Müller and M. Koch-Müller, *Mineral. Mag.*, 2009, **73**, 569–583.
12 M. Shen, M. Huang, Z. Lu and X. He, *RSC Adv.*, 2023, **13**, 25571–25577.
13 B. A. Gaweł, A. Ulvensøen, K. Łukaszuk, B. Arstad, A. M. F. Muggerud and A. Erbe, *RSC Adv.*, 2020, **10**, 29018–29030.
14 J. S. Li, X. X. Li, Q. Shen, Z. Z. Zhang and F. H. Du, *Environ. Sci. Technol.*, 2010, **44**, 7673–7677.
15 K. B. Loritsch and R. D. James, *US Pat.*, US4983370A, 1990.
16 Z. Wei, Y. Li, P. Li, L. Pan, X. Hu, Y. Gu and Y. Tian, *Minerals*, 2023, **13**, 1280.
17 X. Wu, MSc thesis, Southwest University of Science and Technology, 2016.
18 J. Götze, Y. Pan and A. Müller, *Mineral. Mag.*, 2021, **85**, 639–664.
19 B. Lawn, D. Marshall, R. Raj, G. Hirth, T. Page and J. Yeomans, *J. Am. Ceram. Soc.*, 2021, **104**, 23–26.
20 R. A. Young, P. E. Mackie and R. B. Von Dreele, *J. Appl. Crystallogr.*, 1977, **10**, 262–269.
21 A. F. Wright and M. S. Lehmann, *J. Solid State Chem.*, 1981, **36**, 371–380.
22 T. Barth, *Am. J. Sci.*, 1932, **23**, 350–356.
23 W. DOLLASE, *Z. Kristallog.*, 1965, **121**, 369–377.
24 H.-J. Blankenburg, *Quarzrohstoffe*, 1978.
25 J. P. Perdew and Y. Wang, *Phys. Rev. B: Condens. Matter Mater. Phys.*, 1992, **45**, 13244.
26 G. Zhu, Z. Wei, X. Wu and Y. Li, *Sci. Total Environ.*, 2023, **904**, 166273.
27 M. Hong, J. Xu and H. H. Teng, *Geochim. Cosmochim. Acta*, 2016, **172**, 55–64.
28 P. Elstnerová, M. Friák, H. O. Fabritius, L. Lymperakis, T. Hickel, M. Petrov, S. Nikolov, D. Raabe, A. Ziegler, S. Hild and J. Neugebauer, *Acta Biomater.*, 2010, **6**, 4506–4512.
29 M. L. Keith and O. F. Tuttle, *Am. J. Sci.*, 1952, **250**, 203–280.
30 W. H. Baur, *Z. Kristallog.*, 2010, **224**, 580–592.
31 R. D. Shannon, *Acta Crystallogr., Sect. A*, 1976, **32**, 751–767.